JOURNAL OF GUIDANCE, CONTROL, AND DYNAMICS
Vol. 31, No. 3, May–June 2008

Spacecraft Maneuver and Stabilization for Emergency Atmospheric Entry with One Control Torque

Eduardo García-Llama*
GB Tech, Inc., Houston, Texas 77058
and
Juan S. Senent*
Odyssey Space Research LLC, Houston, Texas 77058

DOI: 10.2514/1.31531

This paper presents a method, primarily conceived as an emergency backup system, that addresses the problem of a manned space capsule that needs to execute a safe atmospheric entry from an arbitrary initial attitude and angular rate in the absence of nominal control capability. The proposed concept permits the arrest of a tumbling motion, orientation to the heat-shield-forward position, and the attainment of a ballistic roll rate of a rigid spacecraft with the use of control in one axis only. To show the feasibility of such a concept, the technique of single-input/single-output feedback linearization using the Lie derivative method is employed. The problem is solved for different numbers of jets and for different configurations of the inertia matrix. In the case of an axisymmetric spacecraft, the closed-loop stability is analyzed through the zero dynamics of the internal dynamics. In the cases in which the inertia matrix has cross products of inertia different from zero, the internal dynamics becomes practically intractable. In these cases, only an assessment of closed-loop stability coming from the analysis of different simulation cases is provided. The results show that for the proposed concept and control method to be feasible, a specific geometric layout of the actuators is required for each inertia configuration and number of jets employed in the system.

I. Introduction

THE location and orientation of the reaction control system (RCS) jets in a manned atmospheric entry capsule is arranged to provide control in three axes: that is, torques on pitch, yaw, and roll. At the end of a mission, after separation from the service module (SM), the RCS maneuvers the capsule to the entry attitude and, during nominal atmospheric flight, manages the orientation of the capsule's lift vector to control crossrange and downrange. In the absence of backup systems, a major malfunction in the nominal RCS after the separation from the SM would prevent the capsule from actively recovering from either a possible tumbling or from an adverse attitude that could result in a non-heat-shield-forward entry. The difficulty in attaining a heat-shield-forward attitude before the onset of heat rate levels that could jeopardize the safety of the crew would be higher in entry capsules with two aerodynamic trim angles of attack, as was the case in the Apollo spacecraft, which had a weak trim point close to the apex [1].

To date, the only way to cover for the preceding situation is to add redundant control systems that are similar in logic to the nominal. The Russian *Soyuz* provides redundancy for the roll jets only, making the assumption that the spacecraft is already placed at the right attitude before entry, with very small initial rates [2]; on the other hand, the Apollo capsule had two RCS strings: that is, two complete three-axis control systems, one being the backup of the other [3].

In case a software or hardware failure makes it impossible to fly a guided atmospheric entry, the emergency entry system mode is invoked to fly a ballistic entry. A ballistic entry is solely focused on crew survival. To achieve a safe ballistic entry, two control phases need to be executed sequentially: First, the spacecraft must be oriented such that the heat shield faces the incoming airflow (i.e., in a heat-shield-forward attitude) to counteract the heat rate buildup, and second, the spacecraft must attain a ballistic roll rate during entry to prevent a lift-vector-down situation that would result in excessive loads on the crew.

This paper presents a new backup control concept that, by providing one-axis control with a minimum of one pair of opposed body-fixed backup jets under the constraint of the maximum torque that it can provide, will be able to arrest a tumbling motion, orient the spacecraft's longitudinal axis so the capsule's heat shield is placed in the forward position, force it to remain bounded within a selected total angle of attack θ (angular distance between the longitudinal axis and the direction of the velocity vector), and attain a ballistic roll rate. Furthermore, for a capsule designed to have two complete RCS sets of actuators, the technique proposed in this paper could be included as an emergency last-ditch system that involves little mass addition.

The spacecraft, using the proposed backup technique, constitutes an underactuated system (a system with fewer independent control inputs than degrees of freedom) with nonlinear dynamics. The problem of attitude maneuver and stabilization of a rigid body with one control started to be studied in the 1960s to deal with spin-stabilized bodies, for which the simplest control involves a single thruster at right angles to the spin axis of the satellite or missile. A large roll rate had been given to the body for its stabilization, and the thruster is turned on for fractions of time at each revolution about the spin axis so that the desired attitude changes are achieved. Athans and Falb [4] consider the problem of time-optimal velocity control of a rotating body with a single axis of symmetry. They show that for a single fixed-control jet, the system has the properties of a harmonic oscillator. Thus, a switching curve can be derived to implement the control scheme. The cases of a gimballed control jet and two control jets are also considered. No mention is made of the complete attitude-reorientation problem, however. Other references discuss the problem of reorienting a rotating rigid body with one control [5–14]. However, in all cases, a zero initial transverse angular velocity and a constant roll rate during the control phase are assumed. Jahangir and Howe [15] develop a control scheme to take a missile to some final attitude in minimum time while reducing the transverse angular velocity to zero. Although some arbitrary initial transverse angular velocity is considered in this case, the study assumes, together with a constant roll rate throughout the control phase, a determined initial attitude at which the initial missile-body-axis system coincides with

Received 10 April 2007; revision received 10 July 2007; accepted for publication 26 September 2007.

*Research Engineer. Member AIAA.

the inertial-axis system. Although the results presented in these works are very well suited for spinning bodies, they are not applicable to the case of a tumbling body that needs to achieve a specific orientation of its longitudinal axis, as in the case being considered in this paper.

Aeyels and Szafranski [16] establish that a rigid body can be smoothly stabilized with a linear control law with just one control torque, as long as it is aligned with an axis having a nonzero component along the principal axes and there are no symmetries in the body. Later, it was shown that there exists a nonlinear control law that achieves asymptotic stabilizability for the case in which body symmetries are considered [17]. A control law that stabilizes a uniform rotation of a rigid body about its intermediate axis using a single torque about its major or minor axes was later derived [18,19]. With these results, a single axis control could be designed to stabilize a tumbling body; however, such a control would not be able necessarily to maneuver the vehicle to a desired orientation or to impart a specific roll rate.

As for the controllability when only one actuator is available, Crouch [20] provides the controllability condition for the full state when the jet actuator yields one independent torque. However, that condition does not guarantee taking the system to an equilibrium point. In other words, as mentioned in that paper, the local controllability is not guaranteed. Because our goal is to take a subset of the state to an equilibrium point, Crouch's controllability condition does not apply to the control problem addressed in this paper.

To show the feasibility of the proposed emergency concept, the control technique of single-input/single-output (SISO) feedback linearization using the Lie derivative method is employed [21,22]. Feedback linearization applied to the three-axis attitude control problem has been proposed to deal with cases in which linear approximation assumptions do not apply [23–26]. Feedback linearization applied to underactuated nonlinear spacecraft has only been found in [27], in which the spacecraft model considered had six degrees of freedom, three translational and three rotational, with four control inputs, three of which are for attitude control, resulting in a problem of a different nature from the one dealt with in this paper, because in our case, we are not interested in translation control.

To reorient the spacecraft to the heat-shield-forward position, we need to control one variable only: the total angle of attack. This justifies the feedback being SISO, with the consequence that all the other variables (angular rates and roll angle) will have no control (although they should remain bounded). Nevertheless, all resulting angular rates should comply with medical constraints in the case of a manned vehicle. However, these medical limits are in fact very high in the case of an off-nominal entry [28], ranging from around 450 deg/s during 100 s to 60 deg/s for up to 700 s. We will see that the initial angular rates would have to be of that order to result in similar rates at the end of the control phase. Also, such high initial rates would saturate a reasonable control torque capacity, and therefore such (somewhat unrealistic) severe initial conditions are not going to be considered in this study.

The closed-loop stability of the proposed control on θ will be analyzed for the axisymmetric inertia matrix $I_{xx} > I_{yy} = I_{zz}$, in which it will be shown how two different geometric arrangements of the actuators influence the global closed-loop stability of the system, which will be studied through the zero dynamics of the internal dynamics [21,22]. Also in this case, the trajectories generated by the feedback control loop will be compared with those generated by an optimal indirect method.

Two more inertia configurations will be considered: a realistic complete inertia matrix with $I_{xx} > I_{yy} > I_{zz}$, $I_{ij} \neq 0$ and a partially complete inertia matrix with $I_{xx} > I_{yy} > I_{zz}$, $I_{xz} \neq 0$, with the remaining cross products of inertia equal to zero, representing an intermediate inertia in complexity between the axisymmetric case and the realistic case. In both, the internal dynamics become practically intractable, and therefore the control design will be influenced by the results and guidelines derived from the case of the axisymmetric inertia matrix. The assessments in stability in these two cases will be derived from the experience of running different simulations. It will be shown that specific arrangements of the geometric layout of the actuators will be required for each case.

We will see that in the process of achieving the heat-shield-forward attitude, a roll rate is generated. This roll rate needs to be higher in absolute value than a given ballistic rate. However, a roll rate too high, although complying with the medical criteria, could jeopardize the safe deployment of the landing system. Furthermore, the unintended presence on the spacecraft of even a small rolling aerodynamic moment might result in an unacceptable roll rate from either the ballistic or the landing system standpoint.

These problems lead to the second phase of the control. The proposed solution consists of switching from the control on θ to a control on roll rate ω_x, using the same control technique of SISO feedback linearization and the same set of body-fixed backup jets. Under a control in ω_x, the other variable of interest, the total angle of attack, will have no control. In the absence of atmosphere, this might result in θ losing its heat-shield-forward orientation. Therefore, the transition to control in ω_x must be done in the presence of atmosphere, when the dynamic pressure is sufficiently high as to result in appreciable aerodynamic restoring moments that will tend to trim the capsule in the designed primary trim point in the heat-shield-forward position.

Even though the control on θ can be used in the presence of atmosphere, for the sake of evaluating the control response and its effectiveness in an environment without perturbations, its applicability will be studied in exoatmospheric conditions [between SM separation and entry interface (EI)]. Therefore, for all practical purposes, we will assume zero atmospheric density when analyzing this control phase. Also, the gravitational moments and the rate of change of the flight path angle along the portion of the elliptical orbital trajectory from SM separation to EI are basically negligible and will be ignored.

Throughout the paper, the values used for the different inertia configurations, arms, backup RCS jet thrust levels, and the aerodynamic moment curves will correspond to those of the Apollo entry configuration [1,29]. Presumably, a set of backup jets would have less thrust than the nominal set and would use a different type of fuel and would therefore have a different fuel allotment. A trade analysis on these different possibilities is not going to be addressed in this document, because the main purpose of this paper is to show the feasibility of the proposed emergency backup operational concept.

II. System Equations

The equations describing the control problem are those of a rotating rigid body, with extra terms describing the effect of the control torques. They therefore consist of kinematic equations relating the angular position with the angular velocity and dynamic equations describing the evolution of angular velocity.

A. Dynamic Equations

The dynamics of the rotational motion of a rigid body are described by Euler's equations. Let I be the inertia matrix of the spacecraft, and let $\boldsymbol{\omega}$ denote the angular velocity vector with components along a body-fixed reference frame located at the center of gravity (c.g.) and aligned along the principal axes of the spacecraft. The dynamic equations are presented in Eq. (1), in which $\boldsymbol{ku}$ denotes the control torque vector:

$$I\dot{\boldsymbol{\omega}} = \begin{pmatrix} 0 & \omega_z & -\omega_y \\ -\omega_z & 0 & \omega_x \\ \omega_y & -\omega_x & 0 \end{pmatrix} I\boldsymbol{\omega} + \boldsymbol{ku} = \omega^{\times} I\boldsymbol{\omega} + \boldsymbol{ku} \qquad (1)$$

B. Kinematic Equations

The kinematic equations relate the components of the angular velocity vector with the rates of a set of parameters that describe the relative orientation of two reference frames: an inertial frame and the body-fixed frame. In the formulation of this problem, the inertial frame ($O\hat{X}_V$, $\hat{Y}_V$, and $\hat{Z}_V$) is associated with the velocity vector. It is

defined with its origin located at the c.g. of the spacecraft, with the $\hat{X}_V$ axis pointed along the velocity vector, the $\hat{Y}_V$ axis pointed along the angular momentum of the trajectory, and the $\hat{Z}_V$ axis pointed along $\hat{Y}_V \times \hat{X}_V$. The body-fixed frame ($O\hat{x}$, $\hat{y}$, and $\hat{z}$) is defined by the body axes. In this case, when the rotation angles are zero, the $\hat{x}$ axis goes along the longitudinal axis, aligned with $\hat{X}_V$, being positive toward the heat shield, $\hat{y}$ is aligned with $-\hat{Y}_V$, and $\hat{z}$ is aligned with $\hat{Z}_V$. For convenience, we will consider a 1-3-1 sequence of rotations, which is a type-2 Euler sequence. The rotations involved are φ about $\hat{X}_V$, θ about $\hat{Z}'_V$, and ψ about $\hat{x}$, where $\hat{Z}'_V$ is the resulting $\hat{Z}_V$ after the first rotation. This selection results in the kinematic equations (2):

$$\begin{aligned}\dot{\varphi} &= (-\omega_y \cos\psi + \omega_z \sin\psi)\csc\theta \\ \dot{\theta} &= \omega_y \sin\psi + \omega_z \cos\psi \\ \dot{\psi} &= \omega_x + (\omega_y \cos\psi - \omega_z \sin\psi)\cot\theta\end{aligned} \tag{2}$$

C. Equations of Motion

Combining Eqs. (1) and (2) yields the attitude control problem. We can see that θ, the variable that we want to control first, only depends on ω_y, ω_z, and ψ in the kinematic equations; therefore, the equation for $\dot{\varphi}$ can be ignored. This makes sense because θ, as well as its angular components, angle of attack, and sideslip angle, are invariant to a rotation around the velocity vector. Hence, the equations of motion can be reduced to

$$\begin{aligned}\dot{\boldsymbol{\omega}} &= I^{-1}\omega^{\times} I\boldsymbol{\omega} + I^{-1}\boldsymbol{k}u \\ \dot{\theta} &= \omega_y \sin\psi + \omega_z \cos\psi \\ \dot{\psi} &= \omega_x + (\omega_y \cos\psi - \omega_z \sin\psi)\cot\theta\end{aligned} \tag{3}$$

III. Nonlinear Feedback Algorithm

The system in Eq. (3) can be written in the form of a SISO system:

$$\dot{x} = f(x) + g(x)u \qquad y = h(x) \tag{4}$$

where

$$\begin{aligned}x &= (\omega_x \;\; \omega_y \;\; \omega_z \;\; \theta \;\; \psi)^T \\ f(x) &= \begin{pmatrix} I^{-1}\omega^{\times} I\omega \\ \omega_y \sin\psi + \omega_z \cos\psi \\ \omega_x + (\omega_y \cos\psi - \omega_z \sin\psi)\cot\theta \end{pmatrix} \\ g(x) &= (I^{-1}\boldsymbol{k} \;\; 0 \;\; 0)^T \qquad h(x) = \theta - \theta_d\end{aligned}$$

with $x \in \Re^n$, where n is the system order (5 in our case), f and g are smooth vector fields on $\Re^n$, and h is a smooth nonlinear function, and where θ_d is the desired, or targeted, θ. A large class of SISO nonlinear systems can be made to have linear input–output behavior through a choice of nonlinear state feedback control law that is given with generality by [22]

$$u = \frac{1}{L_g L_f^{\gamma-1} h(x)}[-L_f^{\gamma} h(x) + v]$$

where $L_f h(x)$ and $L_g h(x)$ stand for the Lie derivatives of h with respect to f and g, respectively; γ is the relative degree of the system; and the input v is a scalar that results from the product of the feedback gain vector times the error vector. This control law yields the γth-order linear system from input v to output y: $\mathrm{d}^{\gamma} y/\mathrm{d}t^{\gamma} = v$, where γ is the smallest integer for which $L_g L_f^{i} h(x) \equiv 0\,(i = 0, \ldots, \gamma - 2)$. It is easier to understand γ as the smallest integer for which the control signal appears in $\mathrm{d}^{\gamma} y/\mathrm{d}t^{\gamma}$ for the first time.

By inspection of Eq. (4) we can see that the relative degree γ will depend on the specific form of the product $I^{-1}\boldsymbol{k}$. Therefore, both the inertia matrix and the geometric layout of the jets are the two factors that affect the relative degree of the system. Note that γ can only take the values 2 or 3 (it cannot be 1, because the first derivative of the output, $\dot{\theta}$, never contains the control): it is 2 if the vector $I^{-1}\boldsymbol{k}$ has either its second or third component other than zero, and γ would be 3 if the vector $I^{-1}\boldsymbol{k}$ only had its first component other than zero. A γ higher than 3 is not possible.

A. Normal Form

The relative degree, and hence the product $I^{-1}\boldsymbol{k}$, has important implications in the stability characteristics of the system under control, because the dimension of its internal dynamics is given precisely by $n - \gamma$. When γ is defined and smaller than n, the nonlinear system in Eq. (4) can be transformed into a so-called normal form, which shall allow us to take a formal look at the stability of the system through the notions of internal dynamics and zero dynamics. The normal state becomes

$$\Phi(x) = (\xi_1 \;\; \cdots \;\; \xi_{\gamma} \;\; \eta_1 \;\; \cdots \;\; \eta_{n-\gamma})^T$$

and the normal form of the system can be written as

$$\begin{aligned} \dot{\xi}_1 &= L_f h(x) = \xi_2 & \dot{\eta}_1 &= L_f \eta_1 = q_1(\xi, \eta) \\ \dot{\xi}_2 &= L_f^2 h(x) = \xi_3 & \dot{\eta}_2 &= L_f \eta_2 = q_2(\xi, \eta) \\ &\vdots & &\vdots \\ \dot{\xi}_{\gamma} &= L_f^{\gamma} h(x) + L_g L_f^{\gamma-1} h(x) u & \dot{\eta}_{n-\gamma} &= L_f \eta_{n-\gamma} = q_{n-\gamma}(\xi, \eta) \\ & & h(x) &= \xi_1 \end{aligned} \tag{5}$$

where the vector field η is a solution of the set of partial differential equations:

$$\nabla \eta_j(x) g(x) = 0 \qquad 1 \le j \le n - \gamma \tag{6}$$

To show that the nonlinear system in Eq. (4) can indeed be transformed into the normal form of Eq. (5), we have to show that we can construct a local diffeomorphism $\Phi(x)$ such that Eq. (5) is verified. To show that $\Phi(x)$ is a diffeomorphism, it suffices to show that its Jacobian $\partial\Phi/\partial x$ is invertible; that is, that the gradients $\nabla\xi_i$ and $\nabla\eta_j$ are linearly independent.

B. Internal Dynamics

The internal dynamics associated with the input–output linearization correspond to the last $n - \gamma$ equations of the normal form and they constitute the unobservable part. However, the control must account for the stability of the whole dynamics, and therefore the system will be stable if the internal dynamics remain bounded. To assess the stability of the internal dynamics, we will use the zero dynamics of the system, which are defined as the internal dynamics of the system when its output is kept at zero by the input. As mentioned in [21], the zero dynamics is an intrinsic feature of a nonlinear system that does not depend on the choice of the control law or the desired trajectories.

The constraint that the output h is identically zero in zero dynamics implies that all of its time derivatives are zero. Thus, the corresponding internal dynamics of the system, or zero dynamics, describes a motion restricted to the $n - \gamma$ dimensional manifold defined by $\xi = 0$. Also, for the system to be in zero dynamics, the input control u must be such that h stays at zero. This means that in zero dynamics, the normal form can be written as

$$[\dot{\xi}_1 = 0, \ldots, \dot{\xi}_{\gamma} = 0, \dot{\eta}_1 = q_1(0, \eta), \ldots, \dot{\eta}_{n-\gamma} = q_{n-\gamma}(0, \eta), h = 0]$$

The analysis of the zero dynamics of the internal dynamics will be carried out for the control on θ in the axisymmetric inertia case only. The resulting expressions in the intermediate and realistic inertias are practically intractable. Nonetheless, we will see that useful conclusions from the axisymmetric case can be extended to the other more realistic cases.

C. Control Design on θ

To establish the feedback control loop, the error signal is defined by

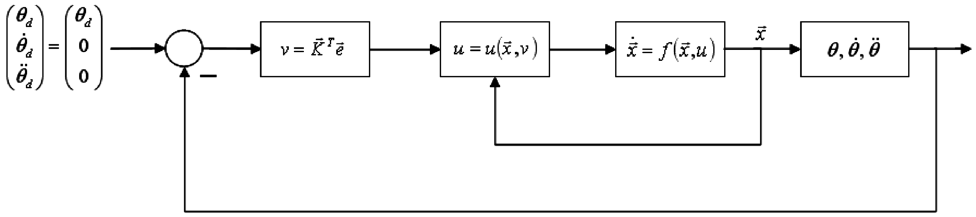

Fig. 1 Control on θ: closed control loop with $\gamma = 3$.

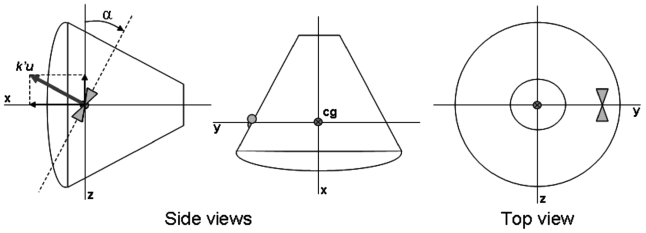

Fig. 2 Axisymmetric inertia matrix; one-axis control torque with components in roll and yaw (two jets).

$$\boldsymbol{e}_{\gamma=3} = (\theta_d, \dot\theta_d, \ddot\theta_d)^T - (\theta, \dot\theta, \ddot\theta)^T$$

or

$$\boldsymbol{e}_{\gamma=2} = (\theta_d, \dot\theta_d)^T - (\theta, \dot\theta)^T$$

depending on whether the relative degree γ is 2 or 3, respectively (note that these are the only two possible values for γ). In both cases, the desired target values of the derivatives of the total angle of attack are zero. The feedback control loop with relative degree 3 is depicted in Fig. 1, in which the feedback gain vector $\boldsymbol{K}$ is such that a desired set of closed-loop pole locations $\boldsymbol{p}$ is matched.

IV. Case with an Axisymmetric Inertia Matrix

In the case of an axisymmetric inertia matrix, we are going to compare two different jet geometry layouts that will result in the only two possible values of the relative degree γ. Because the inertia matrix is a given, the only factor that can determine γ is the vector $\boldsymbol{k}$. A vector $\boldsymbol{k} = (k_x, 0, 0)$, corresponding to a pure roll torque, will result in a nonlinear system with $\gamma = 3$, whereas a vector $\boldsymbol{k}' = (k'_x, 0, k'_z)$, corresponding to a torque with roll and yaw components, will result in a nonlinear system with $\gamma = 2$.

A. Case of Torque with Roll and Yaw Components ($\gamma = 2$)

In the case of a jet layout providing a torque with roll and yaw components (Fig. 2), the term $I^{-1}\boldsymbol{k}'$ is given by

$$I^{-1}\boldsymbol{k}' = \begin{pmatrix} I_{xx}^{-1} & 0 & 0\\ 0 & I_{yy}^{-1} & 0\\ 0 & 0 & I_{zz}^{-1}\end{pmatrix}\begin{pmatrix}\cos\alpha\\ 0\\ -\sin\alpha\end{pmatrix} = \begin{pmatrix} I_{xx}^{-1}\cos\alpha\\ 0\\ -I_{zz}^{-1}\sin\alpha\end{pmatrix} u$$

where α is defined in Fig. 2. The system in Eq. (4) becomes

$$\begin{pmatrix}\dot\omega_x\\ \dot\omega_y\\ \dot\omega_z\\ \dot\theta\\ \dot\psi\end{pmatrix} = \begin{pmatrix} 0\\ a\omega_x\omega_z\\ -a\omega_x\omega_y\\ \omega_y\sin\psi + \omega_z\cos\psi\\ \omega_x + (\omega_y\cos\psi - \omega_z\sin\psi)\cot\theta\end{pmatrix} + \begin{pmatrix} I_{xx}^{-1}\cos\alpha\\ 0\\ -I_{zz}^{-1}\sin\alpha\\ 0\\ 0\end{pmatrix} u$$

$$h(x) = \theta - \theta_d \tag{7}$$

where $a = (1 - I_{xx}/I_{zz})$. The calculation of the necessary Lie derivatives yields the next expression of the control:

$$u = \frac{v - L_f^2\theta}{L_g L_f\theta} = \frac{v - A(\ddot\psi - a\dot\omega_x)}{-I_{zz}^{-1}\sin\alpha\cos\psi} \tag{8}$$

where $A = \omega_y\cos\psi - \omega_z\sin\psi$ and $v = \boldsymbol{K}\cdot\boldsymbol{e}$, with $\boldsymbol{K}$ and $\boldsymbol{e}$ being the feedback gain vector and the error vector, respectively.

Let us now study the stability of this system through the zero dynamics of the internal dynamics. The external part of the normal system will have two components, because $\gamma = 2$, and can be written as

$$\xi_1 = \Phi_1 = h(x) = \theta - \theta_d \qquad \xi_2 = \Phi_2 = L_f h(x) = \dot\theta \qquad \dot\xi_1 = \dot\theta = \xi_2$$

$$\dot\xi_2 = L_f^2 h(x) + L_g L_f h(x) u = A(\ddot\psi - a\dot\omega_x) - I_{zz}^{-1}\sin\alpha\cos\psi u$$

The internal part of the normal system, which will have three components ($n - \gamma = 3$), must satisfy Eq. (6). In this case,

$$g(x) = (I_{xx}^{-1}k'_x \;\; 0 \;\; I_{zz}^{-1}k'_z \;\; 0 \;\; 0)^T$$

thus, Eq. (6) becomes

$$\frac{\partial\eta_1}{\partial x}g(x) = \frac{\partial\eta_1}{\partial\omega_x}I_{xx}^{-1}k'_x + \frac{\partial\eta_1}{\partial\omega_z}I_{zz}^{-1}k'_z = 0$$

$$\frac{\partial\eta_2}{\partial x}g(x) = \frac{\partial\eta_2}{\partial\omega_x}I_{xx}^{-1}k'_x + \frac{\partial\eta_2}{\partial\omega_z}I_{zz}^{-1}k'_z = 0$$

$$\frac{\partial\eta_3}{\partial x}g(x) = \frac{\partial\eta_3}{\partial\omega_x}I_{xx}^{-1}k'_x + \frac{\partial\eta_3}{\partial\omega_z}I_{zz}^{-1}k'_z = 0$$

One possible solution to this system is $\eta_1 = \Phi_3 = \omega_y$, $\eta_2 = \Phi_4 = -k''_z\omega_x + k''_x\omega_z$, and $\eta_3 = \Phi_5 = \psi$, where $k''_x = I_{xx}^{-1}k'_x$ and $k''_z = I_{zz}^{-1}k'_z$. This selection satisfies that $\Phi(x)$ is indeed a diffeomorphism,

$$\operatorname{span}\left(\frac{\partial\Phi(x)}{\partial x}\right) \in \Re^5$$

and we can therefore proceed with the derivation of the internal coordinates:

$$\eta_1 = \omega_y \qquad \eta_2 = -k''_z\omega_x + k''_x\omega_z \qquad \eta_3 = \psi$$

$$\dot\eta_1 = L_f\eta_1 = a\omega_x\omega_z \qquad \dot\eta_2 = L_f\eta_2 = -k''_z a\omega_x\omega_y$$

$$\dot\eta_3 = L_f\eta_3 = \omega_x + (\omega_y\cos\psi - \omega_z\sin\psi)\cot\theta = \omega_x + A\cot\theta = \dot\psi$$

In zero dynamics, we have that $\boldsymbol{e} = 0$ (thus, $v = \boldsymbol{K}\cdot\boldsymbol{e} = 0$) and $L_f^2\theta = \ddot\theta = 0$. These two conditions result in $u = 0$ from Eq. (8). The fact that $u = 0$ in the equations of motion (7) implies that ω_x is constant. Also, the condition that $L_f^2\theta = A(\ddot\psi - a\dot\omega_x) = \dddot\theta = 0$ leads to two possible situations with the same implication: either $A = 0$, which means that $\ddot\psi = \dot\omega_x$ (because $\dot\eta_3 = \omega_x + A\cot\theta = \dot\psi$) or $\dot\psi = a\omega_x$. Both results mean that $\dot\psi$ is constant, because we saw before that ω_x is constant in zero dynamics. Based on these results, we can see that the internal part of the normal system can be written as

$$\dot\eta_1 = c_1\omega_z \qquad \dot\eta_2 = -k''_z c_1\omega_y \qquad \dot\eta_3 = c_2 \text{ or } c_1 \tag{9}$$

where $c_1 = a\omega_x$ and $c_2 = \omega_x$. The internal system (9) is clearly unstable. The component η_3 will not remain bounded for all time, increasing or decreasing indefinitely, depending on the value taken by c_i.

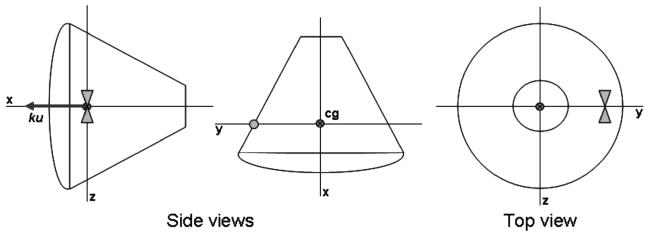

Fig. 3 Axisymmetric inertia matrix; one-axis control torque in roll (two jets).

B. Case with Roll Torque ($\gamma = 3$)

In the case of a jet layout, such as the one depicted in Fig. 3, providing a roll torque, the only difference from the previous case is the term $I^{-1}\boldsymbol{k}$, which is now given by

$$I^{-1}\boldsymbol{k} = \begin{pmatrix} I_{xx}^{-1} & 0 & 0 \\ 0 & I_{yy}^{-1} & 0 \\ 0 & 0 & I_{zz}^{-1} \end{pmatrix} \begin{pmatrix} 1 \\ 0 \\ 0 \end{pmatrix} = \begin{pmatrix} I_{xx}^{-1} \\ 0 \\ 0 \end{pmatrix} u$$

The system in Eq. (4) becomes

$$\begin{pmatrix} \dot{\omega}_x \\ \dot{\omega}_y \\ \dot{\omega}_z \\ \dot{\theta} \\ \dot{\psi} \end{pmatrix} = \begin{pmatrix} 0 \\ a\omega_x\omega_z \\ -a\omega_x\omega_y \\ \omega_y \sin\psi + \omega_z \cos\psi \\ \omega_x + (\omega_y \cos\psi - \omega_z \sin\psi)\cot\theta \end{pmatrix} + \begin{pmatrix} I_{xx}^{-1} \\ 0 \\ 0 \\ 0 \\ 0 \end{pmatrix} u \qquad (10)$$

$$h(x) = \theta - \theta_d$$

where $a = (1 - I_{xx}/I_{zz})$. Calculation of the necessary Lie derivatives yields the next control law:

$$u = \frac{v - L_f^3\theta}{L_g L_f^2 \theta} = \frac{v - \{[2\dot{\psi} - (a+1)\omega_x](a\omega_x - \dot{\psi}) - \dot{\varphi}^2\}\dot{\theta}}{I_{xx}^{-1}(1-a)A} \qquad (11)$$

where $\dot{\varphi}$ from Eq. (2) was introduced to simplify of the control expression.

In studying the stability of this system through the zero dynamics of the internal dynamics, we can see that the external part of the normal system is given by

$$\xi_1 = \Phi_1 = h(x) = \theta - \theta_d \qquad \xi_2 = \Phi_2 = L_f h(x) = \dot{\theta}$$

$$\xi_3 = \Phi_3 = L_f^2 h(x) = \ddot{\theta} \qquad \dot{\xi}_1 = \xi_2 \qquad \dot{\xi}_2 = \xi_3$$

$$\dot{\xi}_3 = [(2\dot{\psi} - (a+1)\omega_x)(a\omega_x - \dot{\psi}) - \dot{\varphi}^2]\dot{\theta} + [I_{xx}^{-1}(1-a)A]u$$

The internal part of the normal system will have two components and must satisfy Eq. (6). In this case, $g(x) = (I_{xx}^{-1} \;\; 0 \;\; 0 \;\; 0 \;\; 0)^T$; thus, Eq. (6) becomes

$$\frac{\partial \eta_1}{\partial x} g(x) = \frac{\partial \eta_1}{\partial \omega_x} I_{xx}^{-1} = 0 \qquad \frac{\partial \eta_2}{\partial x} g(x) = \frac{\partial \eta_2}{\partial \omega_x} I_{xx}^{-1} = 0$$

One solution of the internal system that results in $\Phi(x)$ being a diffeomorphism is given by

$$\eta_1 = \omega_y \qquad \eta_2 = \omega_z \qquad \dot{\eta}_1 = L_f\eta_1 = a\omega_x\omega_z \qquad \dot{\eta}_2 = L_f\eta_2 = -a\omega_x\omega_y$$

In zero dynamics, we have that $\boldsymbol{e} = 0$ (thus, $v = \boldsymbol{K}\cdot\boldsymbol{e} = 0$) and $\dot{\theta} = 0$; hence, $u = 0$ from Eq. (11), which implies that ω_x is constant from the equations of motion. Therefore,

$$\dot{\eta}_1 = \dot{\omega}_y = a\omega_x\omega_z \qquad \dot{\eta}_2 = \dot{\omega}_z = -a\omega_x\omega_y$$

$$\dot{\omega}_y = c_1 \cdot \omega_z \qquad \dot{\omega}_z = -c_1 \cdot \omega_y \qquad (12)$$

where $c_1 = a\omega_x$. This system is stable, although not asymptotically, because its eigenvalues are nonreal.

In conclusion, we have seen that the global closed-loop stability is assured in the case in which a pure roll control torque is provided. The fact that the most stable case is the one with the highest relative degree possible ($\gamma = 3$), and hence with the closest possible value to the system order, is logical, because in the case in which the relative degree equals the system order, there are no internal dynamics.

Note that even though having more than two jets might not constitute an added value for this system as an emergency backup, the option to increase the number of jets from one pair to two pairs, or to as many as desired, is also viable. The only consequence is that the maximum control torque capacity would be multiplied by the existing number of pairs.

C. Test Results with Roll Torque

As indicated in the Introduction, the values of the different parameters involved in the generation of the test results will be those of the Apollo entry configuration. In this case, $I_{xx} = 8064.4$ kg m^2 and

$$I_{yy} = I_{zz} = \frac{I_{yy(\text{Apollo})} + I_{zz(\text{Apollo})}}{2} = 6813.0 \text{ kg m}^2$$

In the Apollo capsule, the distance from the theoretical apex to the c.g. was 2.59 m; therefore, because the x component for the location of the jets corresponds to that of the c.g., the arm will be given by 1.65 m. The thrust of the Apollo RCS jets was 444.82 N (100 lbf); hence, the saturation torque value when we have one pair of jets is $\approx$735 Nm. For convenience, when plotting the test results, the control signal will be expressed as an acceleration ($I_{xx}^{-1}u$) rather than a torque, with the maximum acceleration being 5.16 deg/s^2.

In the case of an axisymmetric inertia matrix the change in the roll rate due to the control affects the frequency of the oscillation of ω_y and ω_z but does not affect the transversal rate $\omega_T = \omega_{T0} = (\omega_y^2 + \omega_z^2)^{1/2}$, where ω_{T0} is the initial transversal rate [30]. Therefore, ω_T cannot be changed during the control process and represents a physical limitation to the maximum angular rate toward the desired total angle of attack. This result also indicates that ω_{T0} must be other than zero for this system to be controlled. For all practical purposes, this is not a tough limitation, because typical rate deadbands on orbit are from -5 to 5 deg/s in all axes and from -2 to 2 deg/s before entry. Also, one probable cause to shut down a nominal RCS is the presence of a stack-on jet, which would impart additional angular rate on the vehicle before being shut down. In any case, we must note that an axisymmetric inertia represents more of an academic case than a real case. More realistic inertia configurations are addressed in later sections. Nevertheless, the fact that ω_T remains constant has important implications in the selection of the settling time in the feedback controller. This time cannot be smaller than the time it would take the system to go from the initial to the final total angle of attack at ω_{T0}. Also, because the presence of initial rates will prevent the system from traveling through the minimum arc, the settling time should be chosen with some margin to avoid a continuous saturation of the controller. Therefore, a settling time $t_s = (2\pi/\omega_{T0})\delta$ is selected, where δ is a factor that represents some percentage of added or subtracted time. Unless said otherwise, $\delta = 1.25$, which represents a 25% time addition. However, note that for all practical purposes, the important time is the one that marks the moment at which θ becomes confined below the capsule's side-wall angle. This time is always smaller than t_s.

For the design of the linear controller, $\boldsymbol{K}$ is calculated using a pole-placement technique. The location of the poles was chosen such that there was no overshoot in θ, at least when the control signal is not saturated. The location of the poles will vary with ω_{T0} in the following manner:

$$p = (-1 \quad -5 \quad -7)5/t_s \qquad (13)$$

Figure 4 presents the results from case 1, in which the initial rates are at the edge of a typical rate deadband limits. Case-1 initial conditions are $\omega_{x0} = 2$ deg/s, $\omega_{y0} = -2$ deg/s, $\omega_{z0} = -2$ deg/s, $\theta_0 = 150$ deg, $\psi_0 = 90$ deg, $\theta_d = 9$ deg, and $t_s = 159.1$ s. Figure 4 is divided in two parts. The left side presents the locus of the positive direction of the spacecraft's longitudinal axis ($+x$ axis)

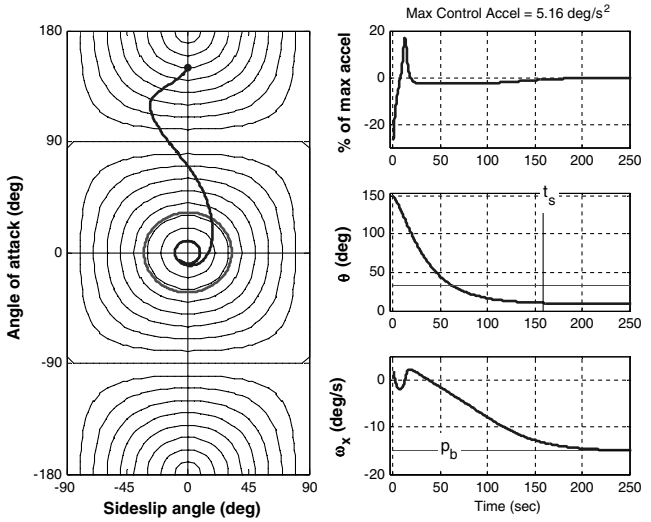

Fig. 4 Axisymmetric inertia matrix; roll control torque; case 1 initial conditions (two jets).

in the projection of the two-dimensional attitude sphere in terms of the angles of attack and sideslip. Each of the contours represents an iso-θ trajectory spaced every 10 deg around the velocity vector, located at the center of the diagram. A spacecraft flying exactly heat-shield-forward would show its locus right at (0,0), whereas a spacecraft flying exactly apex-forward would show its locus at (0 $\pm$180). The ring in the center represents the Apollo side-wall angle (32.5 deg); therefore, as a first approximation, to have the capsule protected from the heat of the entry means that θ should remain confined within that ring. The right side of the chart shows the time histories of the control signal, the total angle of attack, and the roll rate. The control signal is expressed as a percentage of the maximum acceleration that the system can generate. The plot showing θ also indicates the side-wall angle as a straight horizontal line and the settling time t_s, and the roll-rate plot also shows the closest ballistic roll-rate value $\mid p_b \mid$ or $-\mid p_b \mid$, with $p_b = 15\,\text{deg}/s$ for this case.

D. Optimal Control via the Indirect Method

To validate the performance of the proposed nonlinear feedback control, a comparison with an optimal open-loop controller will be provided. The optimal open-loop controller will be calculated using an indirect method. This comparison in performance will be only carried out for the axisymmetric inertia matrix.

The goal of the optimal control law will be to find a minimum torque energy trajectory for a fixed final time $t_f = t_{f_s}$. The selected settling time in the feedback control law t_s will be the final time t_{f_s} in the optimal open-loop control time.

The performance index can be defined as

$$J = \frac{1}{2}\int_0^{t_f} u^2\,\mathrm{d}t$$

The Hamiltonian of this system is defined as

$$H = \frac{1}{2}u^2 + [\lambda_{\omega x}\ \ \lambda_{\omega y}\ \ \lambda_{\omega z}\ \ \lambda_\theta\ \ \lambda_\psi]\begin{bmatrix} I_{xx}^{-1}u \\ a\omega_x\omega_z \\ -a\omega_x\omega_y \\ \omega_y\sin\psi + \omega_z\cos\psi \\ \omega_x + (\omega_y\cos\psi - \omega_z\sin\psi)\cot\theta \end{bmatrix}$$

$$= \frac{1}{2}u^2 + \lambda_{\omega x}I_{xx}^{-1}u + \lambda_{\omega y}a\omega_x\omega_z - \lambda_{\omega z}a\omega_x\omega_y + \lambda_\theta(\omega_y\sin\psi + \omega_z\cos\psi) + \lambda_\psi[\omega_x + (\omega_y\cos\psi - \omega_z\sin\psi)\cot\theta]$$

where λ_i are the costate variables. The costate equation $\dot{\lambda} = -H_x^T(t,x,u,\lambda)$ becomes

$$\dot{\lambda}_{\omega x} = -\frac{\partial H}{\partial \omega_x} = -\lambda_{\omega y}a\omega_z + \lambda_{\omega z}a\omega_y - \lambda_\psi$$

$$\dot{\lambda}_{\omega y} = -\frac{\partial H}{\partial \omega_y} = \lambda_{\omega z}a\omega_x - \lambda_\theta\sin\psi - \lambda_\psi\cos\psi\cot\theta$$

$$\dot{\lambda}_{\omega z} = -\frac{\partial H}{\partial \omega_z} = -\lambda_{\omega y}a\omega_x - \lambda_\theta\cos\psi + \lambda_\psi\sin\psi\cot\theta$$

$$\dot{\lambda}_\theta = -\frac{\partial H}{\partial \theta} = \lambda_\psi(\omega_y\cos\psi - \omega_z\sin\psi)\csc^2\theta$$

$$\dot{\lambda}_\psi = -\frac{\partial H}{\partial \psi} = -\lambda_\theta\omega_y\cos\psi + \lambda_\theta\omega_z\sin\psi + \lambda_\psi(\omega_y\sin\psi + \omega_z\cos\psi)\cot\theta$$

The switching function is obtained from the condition $H_u^T(t,x,u,\lambda) = 0$:

$$\frac{\partial H}{\partial u} = u + \lambda_{\omega x}I_{xx}^{-1} = 0 \Rightarrow u = -\lambda_{\omega x}I_{xx}^{-1}$$

$$u = \begin{cases} -u_{\max} & \text{if } \lambda_{\omega x}I_{xx}^{-1} > +u_{\max} \\ +u_{\max} & \text{if } \lambda_{\omega x}I_{xx}^{-1} < -u_{\max} \\ -\lambda_{\omega x}I_{xx}^{-1} & \text{if } -u_{\max} \le \lambda_{\omega x}I_{xx}^{-1} \le +u_{\max} \end{cases}$$

where $u_{\max}$ and $-u_{\max}$ are the control upper and lower saturation limits, respectively.

The final boundary conditions are given by

$$t_f = t_{f_s}$$
$$x_f = [\text{free}\ \ \text{free}\ \ \text{free}\ \ \theta_d\ \ \text{free}]$$
$$\dot{\theta}_f = 0 \qquad \ddot{\theta}_f = 0$$
$$\lambda_f = G_{x_f}^T(x_f, v)$$

with the endpoint function being

$$G = \nu_1(\theta_f - \theta_d) + \nu_2\dot{\theta}_f + \nu_3\ddot{\theta}_f$$

where ν_i are the Lagrangian multipliers of the endpoint function, and where the subindex f refers to the final value.

Therefore, the components of the final costate vector are given by

$$\begin{aligned} \lambda_{\omega xf} &= \frac{\partial G}{\partial \omega_{xf}} = \nu_3(1-a)A \\ \lambda_{\omega yf} &= \frac{\partial G}{\partial \omega_{yf}} = \nu_2\sin\psi + \nu_3 B\cos\psi \\ \lambda_{\omega zf} &= \frac{\partial G}{\partial \omega_{zf}} = \nu_2\cos\psi - \nu_3 B\sin\psi \\ \lambda_{\theta f} &= \frac{\partial G}{\partial \theta_f} = \nu_1 - \nu_3\frac{A^2}{\sin^2\theta} \\ \lambda_{\psi f} &= \frac{\partial G}{\partial \psi_f} = \nu_2 A - \nu_3 B\dot{\theta} \end{aligned} \tag{14}$$

Because ν_i can take any value, the inspection of system (14) shows that the components $\lambda_{\omega xf}$, $\lambda_{\theta f}$, and $\lambda_{\psi f}$ can be set free, whereas the other two components, $\lambda_{\omega yf}$ and $\lambda_{\omega zf}$, can be expressed in terms of ν_2 and ν_3. From the first and final equations in system (14), we can obtain

$$\nu_2 = \frac{1}{A}\left\{\lambda_{\psi f} + \frac{\lambda_{\omega xf}}{(1-a)A}B\dot{\theta}\right\} \qquad \nu_3 = \frac{\lambda_{\omega xf}}{(1-a)A}$$

where

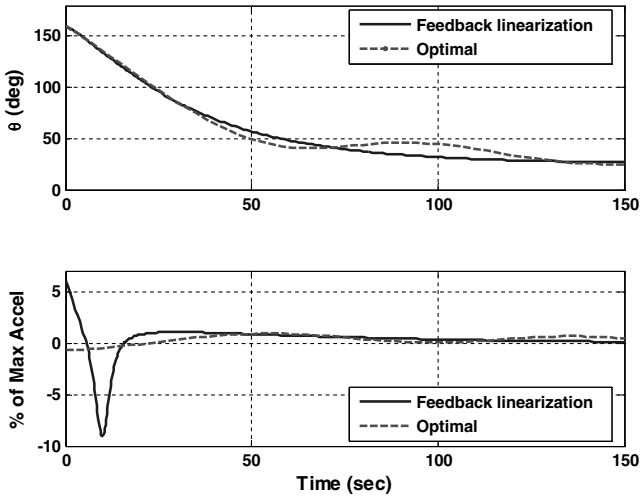

Fig. 5 Axisymmetric inertia matrix; roll control torque; comparison with optimal result.

$$A = \omega_y \cos\psi - \omega_z \sin\psi \qquad B = (1-a)\omega_x + 2A\cot\theta$$

Therefore, the components of the final costate can be expressed as

$$\lambda_{\omega xf} \equiv \text{free} \qquad \lambda_{\theta f} \equiv \text{free} \qquad \lambda_{\psi f} \equiv \text{free}$$

$$\lambda_{\omega yf} = \nu_2 \sin\psi + \nu_3 B\cos\psi \qquad \lambda_{\omega zf} = \nu_2\cos\psi - \nu_3 B\sin\psi$$

In Fig. 5, the time history of θ and the control effort are shown for both control methods.

As expected, the open-loop optimal trajectory requires less control effort [see Eq. (15)]:

$$\begin{aligned} I_{xx}^{-2}\int_0^{t_f} u_{\text{feedback}}^2\,\mathrm{d}t &= 1.22\times10^{-3}\ \text{rad}^2/\text{s}^3 \\ I_{xx}^{-2}\int_0^{t_f} u_{\text{optimal}}^2\,\mathrm{d}t &= 1.37\times10^{-4}\ \text{rad}^2/\text{s}^3 \\ I_{xx}^{-1}\int_0^{t_f} \sqrt{u_{\text{feedback}}^2}\,\mathrm{d}t &= 0.23\ \text{rad/s} \\ I_{xx}^{-1}\int_0^{t_f} \sqrt{u_{\text{optimal}}^2}\,\mathrm{d}t &= 0.12\ \text{rad/s} \end{aligned} \tag{15}$$

The main difference between both time histories is the oscillation that occurs in the trajectory based on optimal control (there is no oscillation in the response of the feedback linearization controller). The selection of nonimaginary poles for the linear controller causes the response to be monotonically decreasing [see Eq. (13)]. Although it would be possible to reduce the cost by selecting poles with imaginary parts and therefore creating oscillations as in the optimal trajectory, it is very difficult to select these poles for an arbitrary set of initial conditions; hence, the selection of poles with no imaginary parts for the linear controller seems interesting from a practical point of view.

V. Case with a Partially Complete Inertia Matrix

In a manned entry capsule, the c.g. location plays a key role in determining its aerodynamic stability and its lift characteristics. The c.g. location is designed to be offset from the centerline to allow for some lift during a nominal atmospheric entry. Otherwise, the capsule would be subject to nominal ballistic entries that would result in high loads on the crew and in the impossibility of having crossrange and downrange control. The main consequence in the inertia matrix of having the c.g. displaced from the centerline (e.g., in the z axis) is that the term I_{xz} turns out to be other than zero.

In this section, we will evaluate what consequences a matrix of the form $I_{xx} > I_{yy} > I_{zz}$, with $I_{xz} \neq 0$, and with the remaining cross products of inertia equal to zero, has in the geometric layout of the actuators. Note that this inertia matrix is very close to a realistic one,

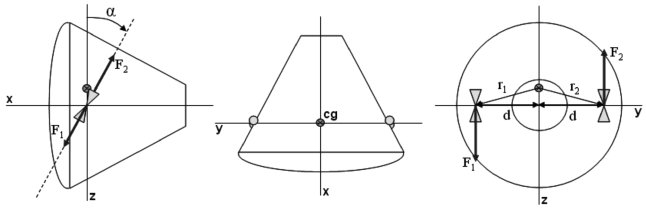

Fig. 6 Partially complete inertia matrix; one-axis control torque with $\gamma = 3$ (four jets).

because the remaining cross products are typically very small compared with I_{xz}. This can be verified by having a look at the inertia matrix of the Apollo entry configuration, where $I_{xx}/I_{xz} = -1/15$, $I_{xx}/I_{xy} = -1/110$, and $I_{xx}/I_{yz} = -1/260$.

In the cases in which the axisymmetric inertia matrix was used, both the closed-loop stability and instability of the internal dynamics (cases with $\gamma = 2$ and 3) could be demonstrated globally. In the current case, the stability of the internal dynamics is practically intractable. However, we have seen in the previous section that a relative degree of 3 ensured the closed-loop stability of the controlled system. Without claiming that having $\gamma = 3$ will ensure stability in this case, we can follow this guideline, assuming that the higher γ is, the more stable the controlled system will be, because there are no internal dynamics when $\gamma = n$ (all cases tested with $\gamma = 2$ resulted in unstable behavior, whereas the cases with $\gamma = 3$ presented instabilities under certain conditions that could be dealt with; these conditions will be shown later). Therefore, we are going to look for the geometric layout of the actuators that results in a controlled system with $\gamma = 3$.

A. Case with Two Pairs of Opposed Jets

Although, as it has been said before, having more than two jets in the proposed emergency backup system does not constitute an advantage, the case in which two pairs of opposed jets are used is included in this section, for completeness, to show how the number of jets affects the geometric layout of the actuators. This layout is presented in Fig. 6, in which $|\boldsymbol{F}_1| = |\boldsymbol{F}_2| \equiv F$, and the total torque is given by

$$\boldsymbol{T} = \sum \boldsymbol{r}_i \times \boldsymbol{F}_i = 2Fd(\cos\alpha, 0, -\sin\alpha)^T$$

which shows that the torque vector is independent of the c.g. offset in the z axis (Z_{cg}). Thus, in this case, $\boldsymbol{k} = (\cos\alpha, 0, -\sin\alpha)^T$, and the term $I^{-1}\boldsymbol{k}$ results:

$$I^{-1}\boldsymbol{k} = \frac{1}{I_{xx}I_{zz} - I_{xz}^2}\begin{pmatrix} I_{zz}\cos\alpha + I_{xz}\sin\alpha \\ 0 \\ -I_{xz}\cos\alpha - I_{xx}\sin\alpha \end{pmatrix}$$

To have $\gamma = 3$, we need to equate to zero the third component of the vector $I^{-1}\boldsymbol{k}$:

$$-I_{xz}\cos\alpha - I_{xx}\sin\alpha = 0 \Rightarrow \alpha_c = \arctan\left\{-\frac{I_{xz}}{I_{xx}}\right\} \tag{16}$$

In the case of the Apollo entry configuration, $\alpha_c \approx 3.73$ deg. Calculation of the necessary Lie derivatives yields the control law, which is not shown here, given its complexity and length.

B. Case with One Pair of Opposed Jets

When we consider the use of one pair of jets instead of two pairs, the achievement of the new jet layout is not as straightforward as in the case of the axisymmetric matrix. If we select the set of jets numbered 1 in Fig. 6, the term $I^{-1}\boldsymbol{k}$ for that set would become

$$I^{-1}\boldsymbol{k} = \frac{1}{I_{xx}I_{zz} - I_{xz}^2}\begin{pmatrix} I_{zz}d\cos\alpha + I_{xz}d\sin\alpha \\ -I_{yy}^{-1}|z_{\text{cg}}|\sin\alpha \\ -I_{xz}d\cos\alpha - I_{xx}d\sin\alpha \end{pmatrix}$$

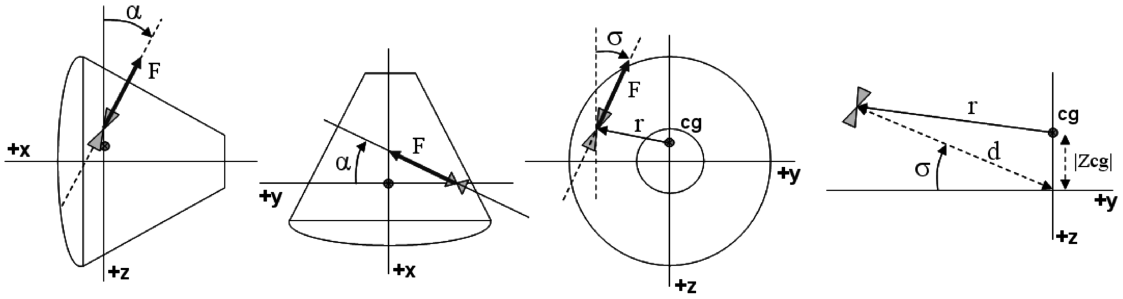

Fig. 7 Partially complete inertia matrix; one-axis control torque with $\gamma = 3$ (two jets).

To obtain $\gamma = 3$, we need to make the second and third components of $I^{-1}\boldsymbol{k}$ equal to zero. In principle, we can see that equating α to zero to have the second component equal to zero leads to having the third component equal to $-I_{xz}d$, hence not resulting in a closed-loop system of relative degree 3. Therefore, to achieve $\gamma = 3$, we need to introduce another degree of freedom in the geometry of the jets' layout. That new degree of freedom will come from a rotation of the location of the actuators around the x axis: σ in Fig. 7. With the geometry depicted in Fig. 7, the torque generated by that set would be given by

$$\boldsymbol{T} = \begin{pmatrix} F\cos\alpha\sin\sigma(-d\sin\sigma + |z_{\text{cg}}|) - F\cos\alpha\cos\sigma(d\cos\sigma) \\ -F\sin\alpha(d\sin\sigma - |z_{\text{cg}}|) \\ F\sin\alpha(d\cos\sigma) \end{pmatrix}$$

and $I^{-1}\boldsymbol{k}$ would become

$$I^{-1}\boldsymbol{k} = \frac{1}{I_{xx}I_{zz} - I_{xz}^2}\begin{pmatrix} I_{zz}\cos\alpha(|z_{\text{cg}}|\sin\sigma - d) - I_{xz}d\sin\alpha\cos\sigma \\ -I_{yy}^{-1}\sin\alpha(|z_{\text{cg}}| - d\sin\sigma) \\ -I_{xz}\cos\alpha(|z_{\text{cg}}|\sin\sigma - d) + I_{xx}d\sin\alpha\cos\sigma \end{pmatrix}$$

To have $\gamma = 3$, we start by equating to zero the second component of $I^{-1}\boldsymbol{k}$ without making $\alpha = 0$:

$$|z_{cg}| - d\sin\sigma = 0 \Rightarrow \sigma_c = \arcsin\left\{\frac{|z_{\text{cg}}|}{d}\right\}$$

We substitute this result into the third component, which must be equated to zero and solved for α, resulting in

$$\alpha_c = \arctan\left\{\frac{I_{xz}(|z_{\text{cg}}|\sin\sigma_c - d)}{I_{xx}d\cos\sigma_c}\right\}$$

In the case of the Apollo entry configuration, $\sigma_c \approx 5.18$ deg and $\alpha_c \approx 3.72$ deg.

C. Test Results

In this section, only a test case with two pairs of opposed jets will be presented. For the partially complete inertia matrix, the values of the inertia elements are $I_{xx} = 8064.4$, $I_{yy} = 7177.7$, $I_{zz} = 6449.6$, and $I_{xz} = -526.1$, all in kg m^2.

Figure 8 shows the results when the initial rates are within typical rate deadbands. Case-2 initial conditions are $\omega_{x0} = 1.5$ deg/s, $\omega_{y0} = 2$ deg/s, $\omega_{z0} = -1.5$ deg/s, $\theta_0 = 160$ deg, $\psi_0 = 350$ deg, $\theta_d = 25$ deg, and $t_s = 180$ s. Unlike in the case of the axisymmetric inertia, where u tended to zero in the time of interest as θ was confined, with the present inertia configuration, the control signal becomes periodic and so do the resulting angular rates. Nevertheless, the control can be turned off at a point at which the conditions are appropriate to ensure the total angle-of-attack confinement and a ballistic entry. Simulation experience shows that acceptable results can be obtained turning off the control when three conditions are met: first, θ has reached θ_d or is close to it; second, the angle of attack is negative; and third, the roll rate is in the ballistic range or close to it. Note that these conditions are found for the present inertia matrix and, in general, should not be extended to other inertia values or

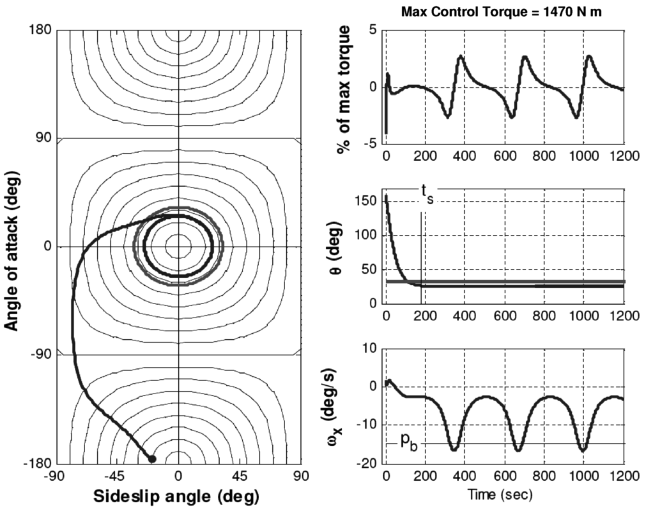

Fig. 8 Partially complete inertia matrix; case 2 initial conditions (four jets).

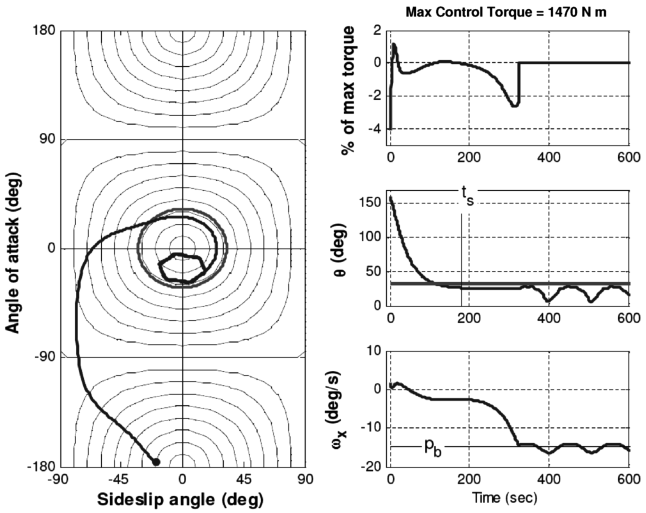

Fig. 9 Partially complete inertia matrix; case 2 initial conditions (four jets); turn-off time is 325 s.

configurations. Thus, if the control is turned off at $t = 325$ s, which is when the preceding conditions are met, we would get the results presented in Fig. 9.

Simulation experience indicates that an element that contributes to making the system unstable is the value of the targeted θ_d. Depending on the initial conditions, a system with a partially complete inertia matrix may become unstable for θ_d smaller than some value θ_{stable}. It was found that, generally, θ_{stable} is between 15 and 20 deg for this particular inertia matrix. For instance, case 2 becomes unstable when $\theta_d = 18$ deg. Therefore, a convenient approach is to set $\theta_d > \theta_{\text{stable}}$.

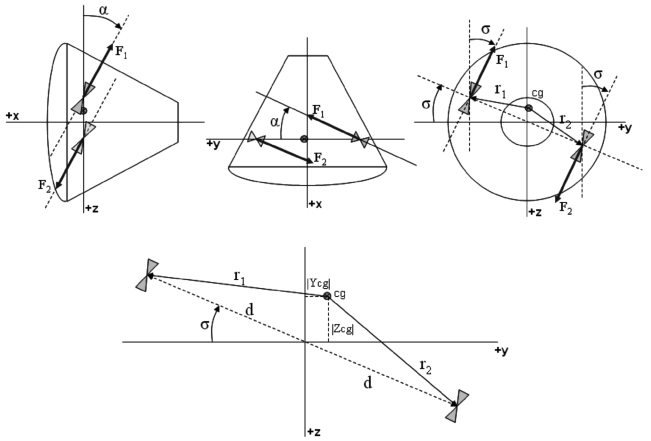

Fig. 10 Complete inertia matrix; one-axis control torque with $\gamma = 3$ (four jets).

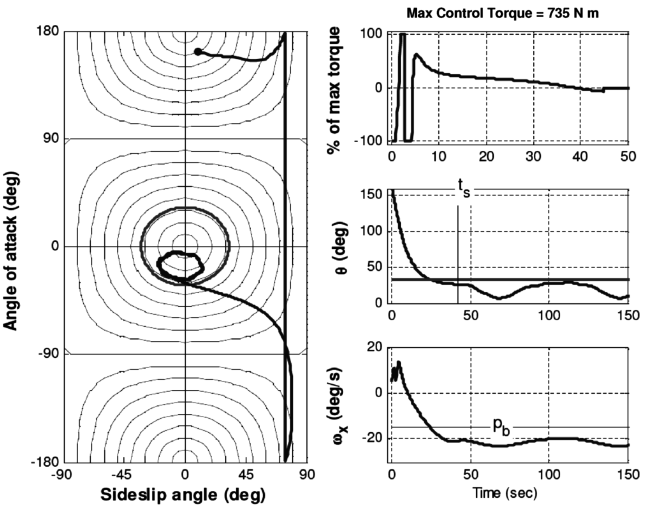

Fig. 11 Complete inertia matrix; case 3 initial conditions (two jets); turn-off time is 45 s.

VI. Case with Complete Inertia Matrix

We are now going to consider the realistic case of a complete inertia matrix ($I_{xx} > I_{yy} > I_{zz}$ with $I_{ij} \neq 0$). To convey a more accurate representation of the actual dynamics, in addition to the complete matrix of inertia and the c.g. offset in the z axis, we are going to account for a displacement of the c.g. in the y axis as well (Y_{cg}); although this displacement is typically of a few tenths of an inch and could be neglected for all practical purposes. Following the guideline from the previous cases, we are going to find a jet's geometric layout that results in a system with relative degree 3 ($\gamma = 3$) for the cases when two pairs and one pair of opposed jets are considered.

A. Case with Two Pairs of Opposed Jets

To have $\gamma = 3$ with two pairs of opposed jets, in addition to having the jets canted with respect to the y–z plane, we will have the locations of both sets of jets rotated about the x axis to have another degree of freedom.

For the jet layout in Fig. 10, with $|\boldsymbol{F}_1| = |\boldsymbol{F}_2| \equiv F$, the torque is given by

$$\boldsymbol{T} = \sum \boldsymbol{r}_i \times \boldsymbol{F}_i = 2Fd(-\cos\alpha, -\sin\alpha\sin\sigma, \sin\alpha\cos\sigma)^T$$

where it can be seen that the torque vector does not depend on either c.g. offset arms. In this case, $\boldsymbol{k}$ has components $k_x = -\cos\alpha$, $k_y = -\sin\alpha\sin\sigma$, and $k_z = \sin\alpha\cos\sigma$. To have $\gamma = 3$, we need to equate to zero the second and third components of $I^{-1}\boldsymbol{k}$. By substituting k_x from the second component of $I^{-1}\boldsymbol{k}$ into its third component, we get

$$k_y = \left(\frac{\text{inv}_{2,3}(\text{inv}_{1,3}/\text{inv}_{1,2}) - \text{inv}_{3,3}}{\text{inv}_{2,3} - (\text{inv}_{1,3}/\text{inv}_{1,2})\text{inv}_{2,2}}\right)k_z$$

$$\Rightarrow \sigma_c = \arctan\left\{-\frac{\text{inv}_{2,3}(\text{inv}_{1,3}/\text{inv}_{1,2}) - \text{inv}_{3,3}}{\text{inv}_{2,3} - (\text{inv}_{1,3}/\text{inv}_{1,2})\text{inv}_{2,2}}\right\} \qquad (17)$$

where $\text{inv}_{i,j}$ represents the elements of the inverse inertia matrix. Substituting this result into the second component of $I^{-1}\boldsymbol{k}$, we get

$$\alpha_c = \arctan\left\{\frac{\text{inv}_{1,2}}{\text{inv}_{2,3}\cos\sigma_c - \text{inv}_{2,2}\sin\sigma_c}\right\} \qquad (18)$$

In the case of the Apollo entry configuration, $\sigma_c \approx -7.78$ deg and $\alpha_c \approx 3.77$ deg. Now $I^{-1}\boldsymbol{k}$ in Eq. (4) becomes

$$I^{-1}\boldsymbol{k} = \begin{pmatrix} -\text{inv}_{1,1}\cos\alpha_c + \sin\alpha_c(\text{inv}_{1,3}\cos\sigma_c - \text{inv}_{1,2}\sin\sigma_c) \\ 0 \\ 0 \end{pmatrix}$$

The stability of the internal dynamics is even more intractable than in the case of the partially complete inertia matrix; therefore, an assessment on stability will be given based on simulation experience.

B. Case with One Pair of Opposed Jets

An arrangement with just two jets can be designed so that $\gamma = 3$. If we select the set of jets numbered 1 in Fig. 10, we can see that $\boldsymbol{k}$ becomes

$$\boldsymbol{k} = \begin{pmatrix} k_x \\ k_y \\ k_z \end{pmatrix} = \begin{pmatrix} \cos\alpha(|z_{cg}|\sin\sigma - |y_{cg}|\cos\sigma - d) \\ -\sin\alpha(d\sin\sigma - |z_{cg}|) \\ \sin\alpha(d\cos\sigma + |y_{cg}|) \end{pmatrix}$$

When this $\boldsymbol{k}$ is used in Eq. (17), the following expression results:

$$\sin\sigma + f^*(\text{inv}_{i,j})\cos\sigma + \frac{|y_{cg}|f^*(\text{inv}_{i,j}) - |z_{cg}|}{d} = 0 \qquad (19)$$

where

$$f^*(\text{inv}_{i,j}) = \frac{\text{inv}_{2,3}(\text{inv}_{1,3}/\text{inv}_{1,2}) - \text{inv}_{3,3}}{\text{inv}_{2,3} - (\text{inv}_{1,3}/\text{inv}_{1,2})\text{inv}_{2,2}}$$

Near $\sigma = 0$, the solution to Eq. (19) for the Apollo entry configuration is $\sigma_c \approx -2.66$ deg. With this value of σ_c, the second component of $I^{-1}\boldsymbol{k}$ must be zero, and the following expression results for α_c:

$$\alpha_c = \arctan\frac{-\text{inv}_{1,2}(|z_{cg}|\sin\sigma_c - |y_{cg}|\cos\sigma_c - d)}{-\text{inv}_{2,2}(d\sin\sigma_c - |z_{cg}|) + \text{inv}_{2,3}(d\cos\sigma_c + |y_{cg}|)}$$

which turns out to be ≈ 3.75 deg in the Apollo entry configuration.

C. Test Results

As it happened in the partially complete inertia matrix case, now the control signal also becomes periodic. Therefore, for practical reasons, we will also have to turn off the control at a point at which the conditions ensure total angle-of-attack confinement to the safe region and the attainment of a ballistic entry. Simulation experience shows that acceptable results can be obtained using the same turn-off conditions described in the case of the partially complete inertia matrix. Also, as in the case of the partially complete inertia matrix, an element that contributes to making the system unstable is the value of the targeted θ_d. Depending on the initial conditions, simulation experience shows that a system may become unstable for a θ_d smaller than some value θ_{stable}. Generally, 15 deg $\leq \theta_{\text{stable}} \leq$ 20 deg. For instance, case 3 becomes unstable when $\theta_d = 15$ deg. As in the case of the partially complete inertia matrix, the possibility of turning off

the control before the onset of the unstable behavior seems to exist in this case too. Again, the best approach would be to select a $\theta_d > 20$ deg.

One representative case when two jets are used is presented in Fig. 11, in which the initial conditions are those of case 3 and the turn-off time is 45 s. Case-3 initial conditions are $\omega_{x0} = 5$ deg/s, $\omega_{y0} = -4$ deg/s, $\omega_{z0} = 10$ deg/s, $\theta_0 = 160$ deg, $\psi_0 = 120$ deg, $\theta_d = 25$ deg, and $t_s = 41.8$ s. The complete inertia matrix of the Apollo entry configuration is given by the following elements: $I_{xx} = 8064.4$, $I_{yy} = 7177.7$, $I_{zz} = 6449.6$, $I_{xz} = -526.1$, $I_{xy} = -71.9$, and $I_{yz} = -31.2$, all in kg m^2.

For the complete inertia matrix configuration, it was found that singularities in the control law prevented the system from being controlled in a number of cases. This aspect of the control algorithm deserves further research.

VII. Inclusion of Atmosphere and Reduction of Final Roll Rate

Up to now, the proposed control concept has been presented only from an exoatmospheric standpoint. The implications when considering different inertia matrices and different numbers of thrusters have been seen, and different methods of dealing with potential unstable or undesired behaviors to ensure an acceptable performance were shown. Nevertheless, should a portion of the control action take place when the spacecraft is traveling through the upper layers of the atmosphere, the demand on the controller would be reduced, due to the spacecraft's aerodynamic restoring moment. This aerodynamic moment will allow for an earlier termination of the control action and for the relaxation of the turn-off conditions.

In the cases in which the initial angular rates are high, the control on θ propitiates a high final roll rate. Even though this final roll rate ensures a ballistic entry and may not violate the crew medical constraints, it may represent a problem at the time to deploy the landing system (drogue and main chutes) later in the flight. This aspect of the crew safety becomes especially important in cases in which the spacecraft has even a small rolling moment C_l. An unintended rolling moment might be present due to protuberances and/or cavities in the outer skin of the spacecraft or due to a nonuniform ablation of the heat shield. Its presence might result in not having the roll rate in the ballistic range or in extreme roll rates at the deployment of the landing system. This is what happened during the unmanned test flight of the Apollo 201, when a pair of electrical short circuits resulted in a loss of power to both of the command modules's independent RCS subsystems, leaving the CM without any means of attitude control. It was later determined that protuberances in the outer skin of the spacecraft resulted in a $C_l = 0.00004$, which spun up the vehicle until chute deployment, when the roll rate was estimated to be over 40 deg/s [31]. In this section, we are going to explore the possibility of controlling the roll rate with the same set of backup jets that were used to place the heat shield forward in the first place.

We have seen that to achieve a relative degree 3 in the control on θ, the jets had to be arranged in a specific geometry, depending on its number and the spacecraft's inertia matrix. Nevertheless, this arrangement has been in all cases, such that the generated torque had its largest component in the longitudinal axis (i.e., x axis or roll axis). An interesting advantage can be extracted from this fact: the possibility of controlling the roll rate through the atmospheric phase of the flight. In the absence of atmosphere, reducing the roll rate implies instability in the total angle of attack and the possible loss of its heat-shield-forward orientation. When the atmosphere is present, the aerodynamic restoring moment greatly compensates this instability.

The analysis will be carried out for just two representative cases: the axisymmetric and the complete inertia matrix configurations, both with the use of just two jets of 444.82 N (100 lbf) each. For simplicity, the effect of the atmosphere in the performance of the jets' thrust is not going to be included in this study. Despite the presence of atmosphere, the system model will basically remain the same as the one presented in Eq. (4). The only difference will reside in the target function $h(x)$, which needs to be modified accordingly, because now the goal is to control ω_x. Now $h(x) = \omega_x^2 - p_b^2$, where p_b is the value of the ballistic roll rate. The squares are selected to ease the handling of the signs, because, in principle, in an emergency situation, it may not matter much whether the spacecraft achieves a positive or a negative ballistic rate. The aerodynamic moments are not included in the system. They will be treated as an unknown perturbation that benefits the control action and will contribute to further confine θ. Also, it is easy to see that the relative degree of our system is now 1, because the control already appears in the first derivative of the variable that we want to control. Unlike in the case when we controlled θ, now the relative degree cannot be altered and the expression for the control becomes $u = (v - L_f\omega_x)/L_g\omega_x$, where the input v results from the product of the feedback gain K times the error e, which are scalars in this case. Therefore, $K = 5/(t_s\delta)$ is now the location of the single closed-loop system's pole, where t_s will have a minimum value possible given by the maximum roll torque that can be generated, and $e = p_b^2 - \omega_x^2$.

In the test results that will be presented next, the atmospheric conditions will be those of an entry from low Earth orbit (LEO) with EI at 121.92 km (4×10^5 ft) and with an initial Earth reference flight path angle $\gamma_r = -1.87$ deg that will be assumed constant. This is a valid approximation, because in a typical LEO entry from that altitude, the flight path angle may vary just about 1 deg during the first 300 s. Other Apollo data that will be used to generate the simulation tests are the reference surface $S_{\text{ref}} = 12.02$ m^2 and the reference length $L_{\text{ref}} = 3.91$ m.

A. Axisymmetric Inertia Matrix with Two Jets

In the case of the axisymmetric matrix, the c.g. is contained in the x axis, and because we are considering a symmetric capsule, the spacecraft will tend to trim at $\theta = \pi/2$ or at $\theta = 0$. In this case, the control law results:

$$u = \frac{v}{2I_{xx}^{-1}\omega_x} = \frac{(p_b^2 - \omega_x^2)}{2I_{xx}^{-1}\omega_x}\frac{5}{t_s\delta}$$

A case that includes the presence of atmosphere and a $C_l = 0.00004$ is presented in Fig. 12. In this case, the initial conditions are $\omega_{x0} = 2$ deg/s, $\omega_{y0} = -10$ deg/s, $\omega_{z0} = -15$ deg/s, $\theta_0 = 150$ deg, $\psi_0 = 90$ deg, $\theta_d = 25$ deg, and $t_s = 25$ s. With these same conditions, if there was no atmosphere, we would see that whereas the roll rate would successfully decrease to the ballistic value, θ would no longer remain confined within the vehicle's side-wall angle. However, with the presence of atmosphere, we can see in Fig. 12 that θ gets more and more confined as the dynamic pressure Q_{bar} is built up, due to the restoring aerodynamic moments.

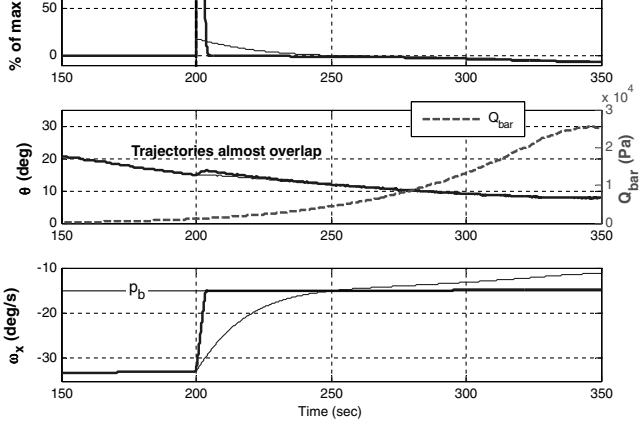

Fig. 12 Axisymmetric inertia matrix (two jets); control on ω_x with atmosphere and $C_l = 0.00004$; control on θ is not shown.

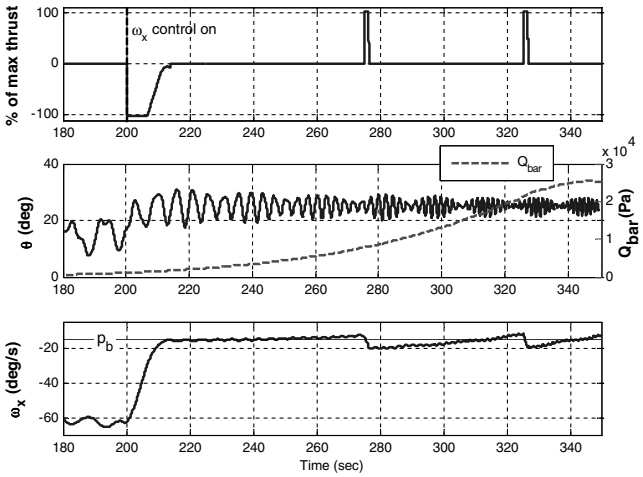

Fig. 13 Complete inertia matrix (two jets); control on ω_x with atmosphere and $C_l = 0.00004$; control on θ is not shown.

When there is atmosphere and $C_l \neq 0$, the effect of a rolling moment can be thought of as a perturbation $p(t)$ that cannot be measured or estimated. If the feedback controller is designed for w_x without taking into consideration the effect of the perturbation, the differential equation that models the tracking error becomes $\dot{e}_{w_x} = Ke_{w_x} + p(t)$. The main consequence is that the long-term (steady-state) tracking error will not be eliminated, but due to the fact that we are mainly interested in reducing the short-term (transient) tracking error and that a very accurate control of w_x is not necessarily required, an increase in the controller gain will reduce the short-term error to acceptable levels. As an alternative, an integral component could be introduced in the controller to improve the long-term tracking error, but this option is not going to be studied in this paper. Figure 12 shows a comparison between having a low feedback gain (with $1/\delta = 0.05$) and a high feedback gain (with $1/\delta = 1$) when the rolling moment is 0.00004.

B. Realistic Inertia Matrix with Two Jets

In the case of the realistic matrix, the c.g. is offset from the x axis. In the Apollo case, the spacecraft has two trim points: at around 25 deg and at around 165.5 deg. The control law on ω_x is not shown, given its length. Only a case with atmosphere and with $C_l = 0.00004$ will be presented. The initial conditions are $\omega_{x0} = 2$ deg/s, $\omega_{y0} = -3$ deg/s, $\omega_{z0} = -5$ deg/s, $\theta_0 = 150$ deg, $\psi_0 = 90$ deg, $\theta_d = 25$ deg, and $t_s = 77.2$ s. In Fig. 13, we can see that the spacecraft is trimming at the right angle of attack (25 deg). The fact that the spacecraft is trimming at that angle while having a roll rate is an indication that the vehicle, as could be expected, is actually banking about the velocity vector at the trim angle of attack. In this case, the control on ω_x was set to zero when the ballistic rate was reached to avoid oscillations on the control signal when it tries to keep the ballistic roll rate constant. The consequence of turning off the control in the case were $C_l \neq 0$ is that the roll rate will deviate from its original value throughout the flight, so that eventual control action will be required to compensate this deviation. Nevertheless, the requirement to fly at the exact ballistic rate is not a hard one, especially in an emergency case, and some error margin around that value should be tolerated. Consequently, the amount of control correction can be adjusted such that its usage is reduced.

VIII. Conclusions

The results presented in this paper show that the proposed emergency backup operational concept for atmospheric entry, producing control in one axis, consisting of a minimum of one pair of opposed body-fixed jets as actuators and an input feedback linearization control system, is capable of maneuvering a spacecraft into a heat-shield-forward position, imparting in the process enough roll rate to achieve a ballistic entry, and controlling the roll rate during the atmospheric flight.

It was shown that for the axisymmetric case with relative degree 3, there exists a feedback control law that can transfer the system to $\theta = \theta_d$ and $\dot{\theta} = \ddot{\theta} = 0$, whereas the rest of the state variables remain bounded. Specifically, ω_x and $\omega_y^2 + \omega_z^2$ remain constant. Also, a feedback control law based on feedback linearization that satisfies the preceding condition was formulated. The controller's gains were designed to depend on the initial conditions and they were generated following a standard pole-placement methodology. For the axisymmetric case with relative degree 2, it was shown that a control law that transfers the system to $\theta = \theta_d$ and $\dot{\theta} = \ddot{\theta} = 0$ will render the system unstable.

It was also shown that to make the relative degree 3, which is the maximum value possible when using only one-axis control torque, the actuators must be arranged in a specific geometric layout that is dependent on the inertia matrix and the number of jets. In the case of the control system on ω_x, the relative degree is 1 and cannot be altered.

Although in the case of an axisymmetric inertia matrix, the closed-loop stability of the system when controlling θ was demonstrated to be globally stable, in the cases of more realistic inertia configurations (although some functional conclusions based on simulation experience were provided), the stability of the closed-loop system is practically intractable, at least when studying the zero output dynamics. Other approaches to global stabilization or, more generally, to the control of nonminimum phase systems have not been investigated in this research and should definitely be subject to future work. However, simulation results show that when a relative degree of 3 is used, a feedback control law succeeds for a wide range of initial conditions.

In the cases of realistic inertia configurations, it was also shown that to maintain θ confined, the control signal becomes periodic. To save fuel, the control on θ can be turned off at a point from which θ will remain confined, and the roll rate will be enough to allow for a ballistic entry. The turn-off conditions were found for the specific inertia matrix used in the study. Although the turn-off conditions are largely relaxed in the presence of atmosphere, the relationship between turn-off conditions and inertia configurations, together with the effect of the atmosphere in those conditions, deserves further investigation.

Acknowledgments

The authors want to thank Christopher J. Cerimele and Lee E. Bryant, respectively, Branch Chief and Deputy Chief for the Flight Mechanics and Trajectory Design Branch at the NASA Johnson Space Center, for their confidence in this work.

References

[1] "Aerodynamic Data Manual for Project Apollo," North American Aviation, Inc., Space and Information Systems Div., TR SID-64-174C, Downey, CA, Jan. 1965.

[2] "Entry Control System: Soyuz TMA Transport Vehicle," Yu. A. Gagarin Russian State Scientific-Research and Test Centre of Cosmonaut Training, TR 03.09.05.T0018, Star City, Russia, 2003.

[3] Taeuber, R. J., and Weary, D. P., "Apollo Experience Report: Command and Service Module Reaction Control Systems," NASA Manned Spacecraft Center TN D-7151, Houston, TX, June 1973.

[4] Athans, M., and Falb, P. L., *Optimal Control*, McGraw–Hill, New York, 1966, pp. 841–853.

[5] Howe, R. M., "Attitude Control of Rockets Using a Single Axis Control Jet," *11th International Astronautical Congress*, Springer, New York, 1961, pp. 88–98.

[6] Windenknecht, T. G., "A Simple System for Sun Orientation of a Spinning Satellite," National IAS-ARS Joint Meeting, Los Angeles, Inst. of the Aerospace Sciences, Paper 61-204-1898, June 1961.

[7] Cole, R. D., Ekstrand, M. E., and O'Neil, M. R., "Attitude Control of Rotating Satellites," *ARS Journal*, Vol. 31, No. 10, 1961, pp. 1446–1447.

[8] Adams, J. J., "Study of An Active Control System for a Spinning Body," NASA TN D-905, June 1961.

[9] Freed, L. E., "Attitude Control System for a Spinning Body," National IAS-ARS Joint Meeting, Los Angeles, Inst. of the Aerospace Sciences, Paper 61-207-1901, June 1961.
[10] Grasshoff, L. H., "A Method for Controlling the Attitude of a Spin-Stabilized Satellite," *ARS Journal*, Vol. 31, No. 5, May 1961, pp. 646–649.
[11] Grubin, C., "Generalized Two-Impulse Scheme for Reorienting a Spin Stabilized Vehicle," *Guidance and Control 2*, edited by R. C. Landford and C. J. Mundo, Progress in Aeronautics and Astronautics, Vol. 13, Academic Press, New York, 1964, pp. 649–668.
[12] Patapoff, H., "Bank Angle Control System for a Spinning Satellite," AIAA Paper 63-339, Aug. 1963.
[13] Wheeler, P. C., "Two-Pulse Attitude Control of an Asymmetric Spinning Satellite," *Guidance and Control II*, Vol. 13, Progress in Astronautics and Aeronautics, AIAA, New York, 1964, pp. 261–287.
[14] Porcelli, G., and Connolly, A., "Optimal Attitude Control of a Spinning Space Body-A Graphical Approach," *IEEE Transactions on Automatic Control*, Vol. 12, No. 3, June 1967, pp. 241–249. doi:10.1109/TAC.1967.1098595
[15] Jahangir, E., and Howe, R. M., "Time-Optimal Attitude Control Scheme for a Spinning Missile," *Journal of Guidance, Control, and Dynamics*, Vol. 16, No. 2, Mar.–Apr. 1993, pp. 346–353.
[16] Aeyels, D., and Szafranski, M., "Comments on the Stabilizability of the Angular Velocity of a Rigid Body," *Systems and Control Letters*, Vol. 10, No. 1, 1988, pp. 35–39. doi:10.1016/0167-6911(88)90037-0
[17] Sontag, E., and Sussmann, H., "Further Comments on the Stabilizability of the Angular Velocity of a Rigid Body," *Systems and Control Letters*, Vol. 12, No. 3, 1989, pp. 213–217. doi:10.1016/0167-6911(89)90052-2
[18] Bloch, A. M., and Mardsen, J. E., "Stabilization of Rigid Body Dynamics by the Energy-Casimir Method," *Systems and Control Letters*, Vol. 14, No. 4, 1990, pp. 341–346. doi:10.1016/0167-6911(90)90055-Y
[19] Aeyels, D., "On Stabilization by Means of the Energy-Casimir Method," *Systems and Control Letters*, Vol. 18, 1992, pp. 325–328. doi:10.1016/0167-6911(92)90021-J
[20] Crouch, P. E., "Spacecraft Attitude Control and Stabilization: Application of Geometric Control Theory to Rigid Body Models," *IEEE Transactions on Automatic Control*, Vol. 29, No. 4, 1984, pp. 321–331. doi:10.1109/TAC.1984.1103519
[21] Weiping Li, and Jean-Jacques E. Slotine, *Applied Nonlinear Control*, Prentice–Hall, Englewood Cliffs, NJ, 1991.
[22] Shankar Sastry, *Nonlinear Systems: Analysis, Stability, and Control*, Springer, New York, 1999.
[23] Sheen, J., and Bishop, R., "Spacecraft Nonlinear Control," *Proceedings of the 1992 AAS/AIAA Spaceflight Mechanics Meeting*, AIAA, Washington, DC, 24–26 Feb. 1992, pp. 613–632.
[24] Lin, Y. Y., "Parameter Space Design of Nonlinear Feedback Control for Spacecraft Reorientation," AIAA Guidance, Navigation and Control Conference and Exhibit, Montreal, Canada, AIAA Paper 01-4157, 6–9 Aug. 2001.
[25] Jensen, H-C. B., and Wiśniewski, R., "Quaternion Feedback Control for Rigid-Body Spacecraft," AIAA Guidance, Navigation and Control Conference and Exhibit, Montreal, Canada, AIAA Paper 01-4338, 6–9 Aug. 2001.
[26] Bang, H., Myung, H.-S., and Tahk, M.-J., "Nonlinear Momentum Transfer Control of Spacecraft by Feedback Linearization," *Journal of Spacecraft and Rockets*, Vol. 39, No. 6, Nov.–Dec. 2002, pp. 866–873.
[27] Fang, B., and Kelkar, A. G., "On Feedback Linearization of Underactuated Nonlinear Spacecraft Dynamics," *Proceedings of the 40th IEEE Conference on Decision and Control*, Vol. 4, Inst. of Electrical and Electronics Engineers, Piscataway, NJ, Dec. 2001, pp. 3400–3405.
[28] William, P. E., and Jacobs, A., "Orbital Space Plane: Level 2 System Requirements Document," NASA Marshall Space Flight Center TR MSFC-RQMT-3360, Huntsville, AL, Nov. 2003.
[29] Low, G. M., and Maynard, W. E., "CSM/LM Spacecraft Operational Data Book - Mass Properties," NASA Manned Spacecraft Center TR SNA-8-D-027, Houston, TX, Apr. 1971.
[30] Wertz, James, R., *Spacecraft Attitude Determination and Control*, Kluwer Academic, Dordrecht, The Netherlands, 1990, pp. 524–525.
[31] "Postlaunch Report for Mission AS-201 (Apollo Spacecraft 009)," NASA Manned Spacecraft Center TM-X-72334, Houston, TX, 6 May 1966.